Article

Physicochemical Characterization and Antibacterial Activity of Titanium/Shellac-Coated Hydroxyapatite Composites

Widyanita Harwijayanti, Ubaidillah Ubaidillah *⬤ and Joko Triyono *

Mechanical Engineering Department, Faculty of Engineering, Universitas Sebelas Maret, Jalan Ir. Sutami 36A, Kentingan, Surakarta 57126, Indonesia; widyanitaharw@student.uns.ac.id
* Correspondence: ubaidillah_ft@staff.uns.ac.id (U.U.); jokotriyono@staff.uns.ac.id (J.T.)

Abstract: Titanium and hydroxyapatite are widely used as materials for implants. Titanium has good mechanical properties, good corrosion resistance, and a high modulus of elasticity. Hydroxyapatite has good biocompatibility, bioactivity, and significant osteoinductivity. In this study, powder metallurgy was used as a method to combine titanium and hydroxyapatite for use in implants. Shellac was used as a binder between ceramic and metal due to its lower melting point. The surface morphology and chemical properties were evaluated by scanning electron microscopy–energy dispersive X-ray (SEM-EDX), whereby the SEM revealed the appearance of micropores in the Ti-HA composites during the sintering process, and the EDX showed that the final product had high amounts of Ti and Ca and low P. X-ray diffraction (XRD) and Fourier transform infrared (FTIR) analyses were used to achieve the chemical characterization of composites, whereby a weak diffraction peak was observed in the XRD spectrum of Ti-HA composites, and the FTIR analysis confirmed that the composites had carbonate $(CO_3)^{2-}$, phosphate $(PO_4)^{3-}$, and hydroxyl $(OH)^{-}$ groups. Oxygen was sufficient due to the sintering process being conducted in an air environment. The antibacterial activities were characterized using the disc diffusion method with *Escherichia coli* and *Staphylococcus aureus* bacteria, whereby the prepared Ti-HA composites had a greater antibacterial effect on *E. coli* than on *S. aureus*. Finally, pH changes were observed during the 24 h incubation. The result showed that the Ti-HA composite did not contain chemical compounds that could cause harmful effects for humans and had good antibacterial activity against *E. coli*.

Keywords: composite; shellac; physicochemical; antibacterial activities

1. Introduction

Dental injuries are found in a significant proportion of the world's population; these injuries represent 5% of all injuries, and up to 17% occur in children [1]. The causes of dental injuries include falling down, sports activities, and traffic accidents. Dental injuries are most commonly found in the front teeth of the upper jaw [2]. The loss of anterior or front teeth affects aesthetics, while the loss of posterior back teeth causes problems when consuming food. If ignored, these problems will lead to other complications, such as headaches, joint problems when chewing, extrusion, and the reduction of tooth size [3]. Population growth has caused an increasing demand for implant materials for bone dysfunction. Implants are needed in order to repair or change bone tissue [4]. For orthopedic and dental implant applications, materials should be biocompatible, have a similar stiffness to human bones, and be resistant to corrosion and fatigue [5]. Long-lived implant materials are necessary for orthopedic and dental implants to reduce the need for repeated surgeries [6].

In recent decades, titanium has been widely used as an implant material because it has good mechanical properties, corrosion resistance, and a high modulus of elasticity but poor biocompatibility [4]. As a material for implants in its solid form, titanium suffers from unsuitable biomechanics, host tissue stability issues, and stress shielding between titanium

and human bones [7]. Thus, the modification of metal materials using bioactive materials is required to reduce the modulus of elasticity and improve biocompatibility.

Hydroxyapatite is a bioceramic calcium apatite with the chemical structure $Ca_{10}(PO_4)_6(OH)_2$ and a 1.67 ratio of Ca/P [8]. Hydroxyapatite has been widely used as a bone substitute for treating bone defect injuries and in bone tissue engineering in addition to being used as a coating for metal implant materials because of its good biocompatibility, bioactivity, and bioconductivity [9]. Hydroxyapatite has an empty area in its structure and can be modified by cationic or anionic substitutions so that it has good adsorption properties and also the ability to bind compounds on the surface [10].

Titanium compounds containing hydroxyapatite can be used as implant materials—for example, in dental implants. Dental implants are the optimal treatment in cases of lost teeth [3]. Commercial dental implant materials are made of a single component and are sometimes coated with a material that shows good compatibility. However, such implant materials cause stress shielding problems around the bone after a certain time [11]. Dislodgement of the ceramic coating on metallic materials due to poor adhesion can lead to the failure of the material implant [12]. To avoid failure in the coating process, a number of studies have been carried out by combining specific properties of some components by forming composite material. The characteristics of composites can be modified to expand their potential use by selecting the synthesis route [10].

Powder metallurgy is a simple method by which titanium powder and hydroxyapatite powder are used to produce composite materials. The challenge in powder metallurgy processes is to combine two or more powders with different sizes and types, along with thermal coefficients. The presence of a binder as an adhesive is needed to increase the ability of powders under high loading conditions [13]. Adhesive additives are needed to combine metal with ceramic to produce a composite. Shellac is a natural biopolymer that can be obtained from lac insects, which are found in Asian countries. Shellac consists of resin, dye, insect wax, and impurities from host trees [5]. Recently, shellac has been used in various fields because of its low toxicity [14].

Hydroxyapatite undergoes a dehydroxylation and decomposition process when sintered above 800 °C in the presence of titanium [15]. Hydroxyapatite has shown antibacterial activity and a zone of inhibition (ZOI) when assayed using *Escherichia coli* and *Staphylococcus aureus* [16]. In another study, Ashraf et al. [17] reported that a titanium oxide (TiO_2) composite had better antibacterial activity against *Escherichia coli* than against *Staphylococcus aureus* [17]. Shellac-coated hydroxyapatite from bovine bone has a Ca/P ratio similar to that of human bone after the calcination process [18]. Shellac is a polymer with low crystallinity and has a melting point between 50 and 75 °C [5]. However, previous studies have not tested using shellac as a binder for powder comprising a combination of titanium and hydroxyapatite.

The aim of this study was to prepare a composite of titanium and hydroxyapatite by sintering at 800 °C using shellac as a binder and evaluate its physicochemical characteristics. Moreover, the antibacterial activity of the composite was investigated using *Escherichia coli* and *Staphylococcus aureus* bacterial strains.

2. Experimental Section

2.1. Preparation of Materials

In this study, powders of hydroxyapatite (Bio World, Dublin, OH, USA) and titanium (Thermo Scientific, Waltham, MA, USA) with microscopic sized particles characterized by irregular shapes were used as starting materials. Shellac solution was used as a coating for hydroxyapatite powder. Shellac was prepared by dissolving shellac powder, which was obtained from lac flea secretions, into alcohol 96% in a glass beaker using magnetic stirring for 1 h. Hydroxyapatite powder, at either 20 vol% or 30 vol%, was then soaked in the shellac solution for 24 h to coat the grains. Titanium powder, at either 80 vol% or 70 vol%, was then mixed into the glass beaker and stirred for 1 h for homogenization.

The mixed powder was left to dry in the sun until a precipitate powder was obtained. The dry mixed powder was compacted in a stainless-steel mold using a hydraulic press at 75 MPa. The green specimen was sintered using a muffle furnace at 800 °C with various holding times, including 3, 4, and 5 h. The preparation scheme for the Ti-HA composites can be seen in Figure 1.
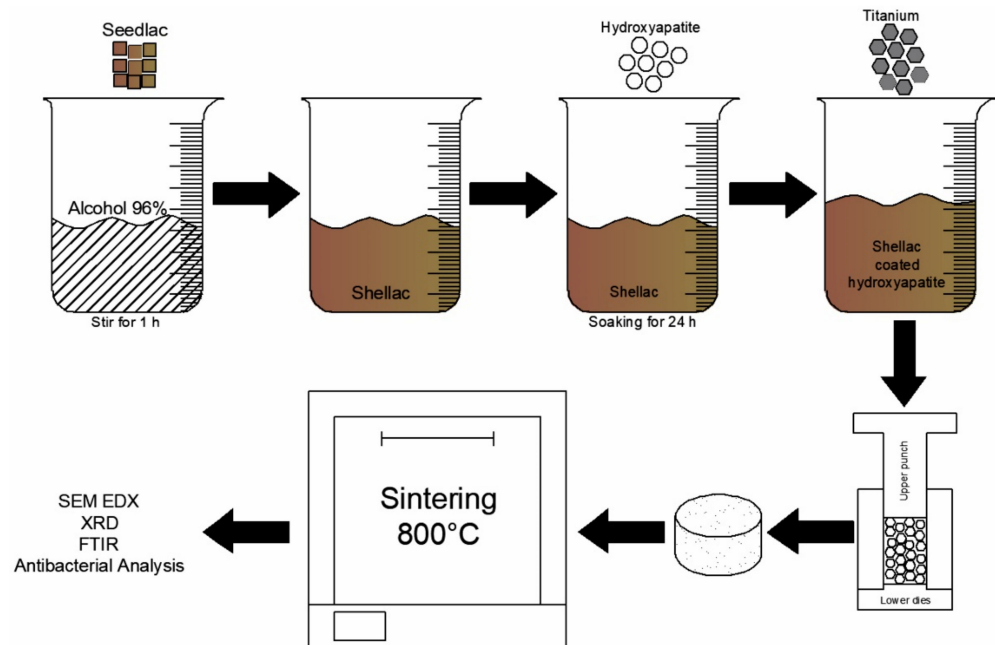

Figure 1. Ti-HA composite sample preparation.

The sintered specimens were analyzed using X-ray diffraction (XRD), Fourier transform infrared (FTIR), and scanning electron microscopy–energy dispersive X-ray (SEM-EDX) analyses, and the antibacterial activities were determined through characterization of the zones of inhibition resulting from the titanium/hydroxyapatite composites. The various samples that were prepared and the relevant preparation details can be seen in Table 1.

Table 1. Samples of varying Ti:HA compositions and their holding times of sintering.

Sample	Ti:HA Composition (*v/v*)%	Sintering Temperature (°C)	Sintering Time (h)
S1	80:20	800	3
S2	80:20	800	4
S3	80:20	800	5
S4	70:30	800	3
S5	70:30	800	4
S6	70:30	800	5

2.2. Characterization

XRD analysis was carried out using an XRD Mini Diffractometer MD10 (MTI Corp., Yeosu, South Joella, Korea) (10 W; 25 kV; 0.4 mA) and an X-ray tube with Cu as an anode; the measuring range of 2θ was 17°–76°. The XRD samples were the starting materials used for the preparation of composites in addition to the six samples prepared under different conditions (Table 1). FTIR analysis was carried out at wavenumbers 650–4000 cm^{-1} using a Cary 630 FTIR Spectrometer (Agilent Technologies Inc., Santa Clara, CA, USA). The surface morphology of the composite was determined using a JCM-7000 Neo Scope Benchtop SEM (JEOL Ltd., Akishima, Japan), 15 kV, with 300× magnification in high-vacuum conditions.

2.3. Antibacterial Activity

To evaluate the antibacterial activities of the composites, the Kirby–Bauer disc diffusion method was used to determine the inhibition zone of bacterial growth. *Escherichia coli* (ATCC25922), as a Gram-positive bacterium, and *Staphylococcus aureus* (ATCC 25923), as a Gram-negative bacterium, were sourced from Laboratorium Terpadu, Universitas Sebelas Maret, Indonesia. These were chosen because they are typical microorganisms implicated in infection in clinical settings [19]. First, 20 mL of Mueller–Hinton Agar (MHA) medium was poured into a Petri dish. The Petri dish was cooled in a refrigerator for 2×24 h to solidify [20]. A bacterial colony was inoculated into a 5 mL nutrient agar (NA) medium with an initial concentration of 1.5×10^8 CFU (colony-forming unit)/mL for 2×24 h. The bacterial inoculum was dissolved with sterile aquadest into the bacterial suspension. The turbidity was adjusted using a 0.5 McFarland standard [16]. The bacterial suspension was swabbed using a sterile cotton bud and the slant culture method by scratching in a zig-zag pattern across the entire surface of the MHA medium. Sterile disc paper 6 mm in diameter was placed onto the Petri dish. The composite titanium/hydroxyapatite powder was dripped onto the paper disc at a concentration of 100 mg/mL. A blank disc was used as a negative control, and a chloramphenicol disc was used as a positive control. The Petri dishes were incubated at 37 °C for 24 h. The bacterial inhibition zone was measured in millimeters (mm) using Vernier calipers. This antibacterial activity analysis was conducted in triplicate ($n = 3$), and the results are represented as means with standard deviation.

3. Results and Discussion

3.1. Physicochemical Characteristics

Figure 2 shows the XRD patterns of titanium powder, hydroxyapatite powder, and shellac. The XRD pattern of titanium consists of an α-Ti phase. Hydroxyapatite, with the chemical structure $Ca_{10}(PO_4)_6(OH)_2$, has high crystallinity, which is confirmed by sharp peaks [21].
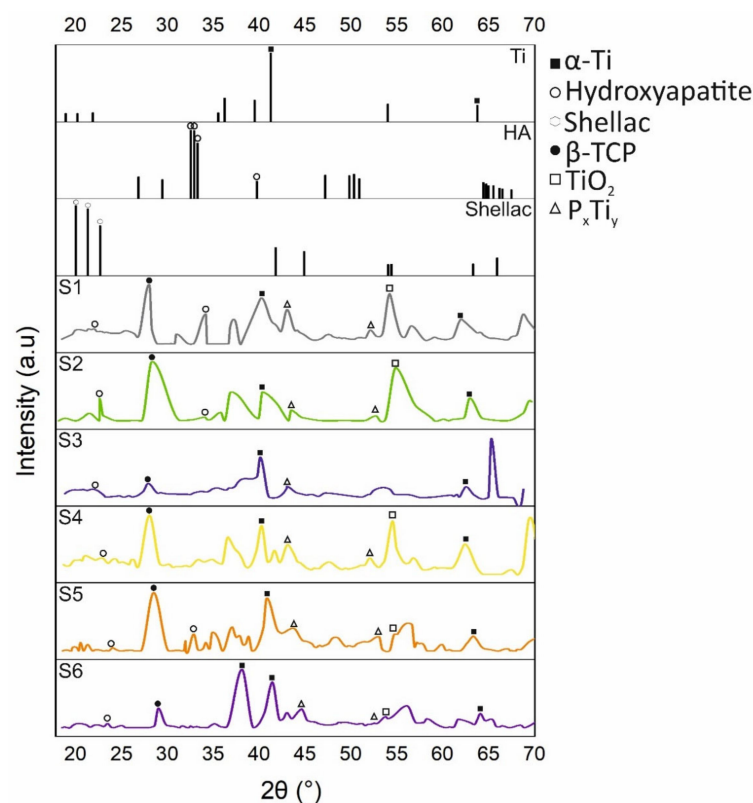

Figure 2. XRD patterns of the initial materials (titanium; hydroxyapatite; shellac) and the Ti-HA composites (S1–S6).

Commercially sourced pure hydroxyapatite powder had two intensity peaks with (*h k l*) values of (2 1 1) and (3 0 0), which are in accordance with the JCPDS Card 09-0432, and commercially sourced pure titanium powder had (*h k l*) values of (1 0 1) and (1 0 0), as in the JCPDS Card 44-1294 [22]. In this experiment, shellac was used as an adhesive for the powders. Shellac is a natural resin that was obtained, in this case, from lac flea secretions. Shellac was dissolved in alcohol 96% to produce a shellac solution that could be used for binding particles. The shellac solution had a concentration of 100 mg/mL. Shellac had two peak intensities at $2\theta = 19.21°$ and $20.55°$. These peaks show that the shellac was in an amorphous phase state [23]. The crystallite size of the composite Ti-HA can be defined by the Scherrer Equation:

$$D = \frac{k\lambda}{\beta \, cos\alpha} \tag{1}$$

where D is the crystal size, λ is the lengthwave of X-ray, β is the full width at half maximum of the peak in radians, and α is the Bragg angle; s in radians [24]. The size of the crystalline Ti-HA composite is shown in Table 2.

Table 2. Mean crystallite size of the Ti:HA composite.

Ti-HA Composite Sample	Crystallite Size (nm)
S1	13.5
S2	22.2
S3	27.3
S4	18.7
S5	14.7
S6	10.7

Figure 2 shows XRD patterns from six experimental composites. The intensity peaks of titanium were identified at 2θ in the range of $40°$, and hydroxyapatite had high crystallinity at $2\theta = 31°–34°$ [15]. Phosphorus (P) ions from hydroxyapatite formed a new chemical structure, P_xTi_y, with titanium [25]. Meanwhile, α-Ti appeared as the main phase of titanium in the titanium/hydroxyapatite composite after the sintering process [6]. Titanium oxide (TiO_2) was observed, which shows there was interaction between the titanium (Ti) and the oxygen (O) from the hydroxyapatite powder. This phase within the composite results from the commonly occurring interaction between titanium and hydroxyapatite [22].

Shellac was analyzed by FTIR to confirm the functional groups present. Figure 3 shows the FTIR spectra of shellac. The shellac peaks at 2964 and 2840 cm^{-1} are due to C-H aliphatic stretching from $-CH_2^-$ and $-CH_3^-$, the peak at 1690 cm^{-1} is due to C=O stretching from -COOH, the peak at 1644 cm^{-1} is due to C=C stretching [5], the peak at 1252 cm^{-1} is due to O-H bending in a hydroxyl group, and the peak at 1158 cm^{-1} is due to C-O stretching in a carbonate group [26]. Carbonate groups were also observed in the 800–900 cm^{-1} and 1350–1600 cm^{-1} regions [27].

Figure 3 also shows the FTIR spectra of the Ti-HA composites. Phosphate groups $(PO_4)^{3-}$ appeared at peaks of 960 and 1033 cm^{-1} [28]. Hydroxyl groups were observed in the 3570–3650 cm^{-1} region. The peak at 2250 cm^{-1} is due to O-H stretching of the hydroxyl groups [29]. The peaks at 870 cm^{-1} and between 1420 and 1476 cm^{-1} are due to the carbonate groups of the $CaCO_3$ phase [30]. The composites showed infrared spectra similar to those of their initial materials but with weaker peaks. This difference occurred due to the dehydroxylation and decomposition process of hydroxyapatite after sintering [31], where several of the peaks of the composites changed after sintering at 800 °C. The hydroxyl groups from hydroxyapatite also decreased with increasing sintering temperatures [30].
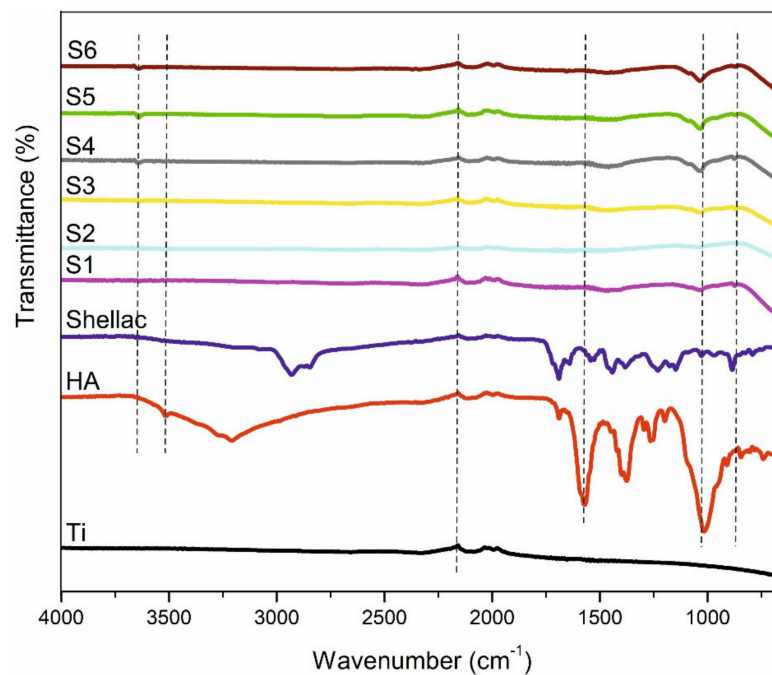
Figure 3. FT-IR spectra of the initial materials (titanium; hydroxyapatite; shellac) and the Ti-HA composites (S1–S6).

The FTIR spectra in the 800–920 cm^{-1} region correspond to carbonate groups that were substituted as v_2 CO$_3$, both of type A and of type B and non-apatitic [32]. Figure 4 shows the deconvolution of Ti-HA composites in the 860–890 cm^{-1} region. The positions of the carbonate groups, which are not easily determined, can be identified using Gaussian curve fitting and the positions of the peaks that appeared by deconvolution [32]. The peak region around 860–890 cm^{-1}, corresponding to the carbonate group, can be deconvoluted into three peaks using Equation (2).

$$Y = \frac{A}{w}\sqrt{\frac{4\ln 2}{\pi}}\,\frac{1}{4\ln 2}\,\frac{(x-xc)^2}{w^2} \tag{2}$$

where A is the area, w is the full width of the graph, and xc is the center [33].

When carbonate groups encounter OH$^-$ groups, type A substitutions will be obtained, whereas when carbonate groups join with PO$_4{}^{3-}$, type B substitutions will be generated [34]. Type A substitutions are indicated by a peak at 880 cm^{-1}, and type B substitutions are indicated by a peak at 875 cm^{-1} [35]. Meanwhile, non-apatitic structures are more soluble and less stable than hydroxyapatite and can easily be transformed into apatite or replaced to calcium phosphate through a wet-method process [36]. Carbonate can also be converted into another type of structure via different drying methods [32].

The composites were prepared by soaking hydroxyapatite powder in shellac solutions for 24 h to coat the particles. Figure 5a shows the SEM of shellac-coated hydroxyapatite. Hydroxyapatite had a spherical morphology with a thin layer appearance after soaking in shellac. The aim of the process was to coat hydroxyapatite so that it could bind another particle, namely, titanium powder. Hydroxyapatite and titanium were mixed using the wet-precipitation method and magnetic stirring for 1 h.
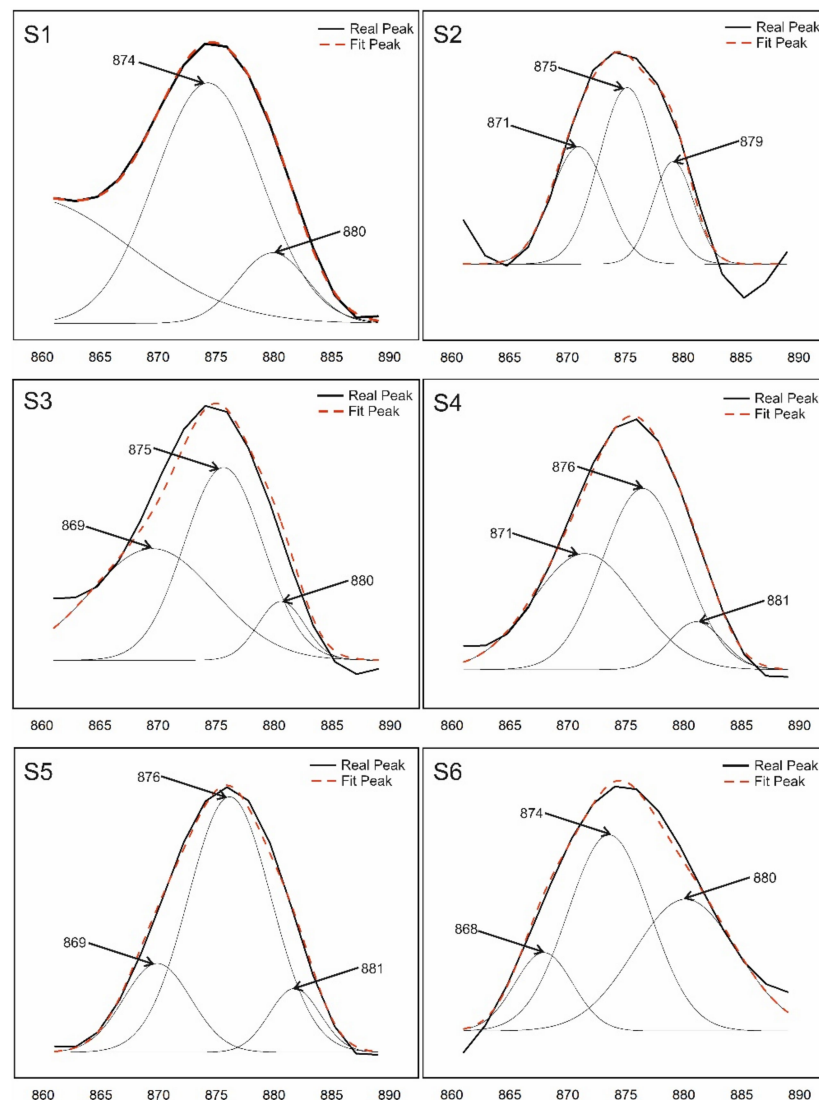
Figure 4. Deconvolution region at 800–920 cm^{-1} for carbonate groups of the Ti-HA composites (S1–S6).

The surface morphology of the composites can also be seen in Figure 5, where the irregular morphology of the titanium particles after the mixing process when using the wet-precipitation method is observed [37]. The dark zone corresponds to porosity during the sintering process. Micropores caused by necking during sintering were observed in the composite surfaces [21].

Agglomerations between the titanium and hydroxyapatite were also seen after composite sintering. The fine agglomeration of the hydroxyapatite was easily broken by uniform pressure during compaction using a hydraulic machine [22]. After compaction and sintering, the composites showed inhomogeneous particle distribution caused by the differences in particle size between titanium and hydroxyapatite and also by the pressure used during compaction [38]. The large amount of titanium was confirmed by EDX analysis, as shown in Figure 5c,g. The Ti-HA composites showed an amount in accordance with the initial ratio used in mixing. EDX analysis showed high amounts of Ti and Ca with low amounts of P. The appearance of oxygen was due to the sintering process, which was carried out in an air environment. Titanium bonds with oxygen during sintering and forms a TiO$_2$ phase [4]. The appearance of TiO$_2$ was confirmed by the XRD spectra shown in Figure 1.
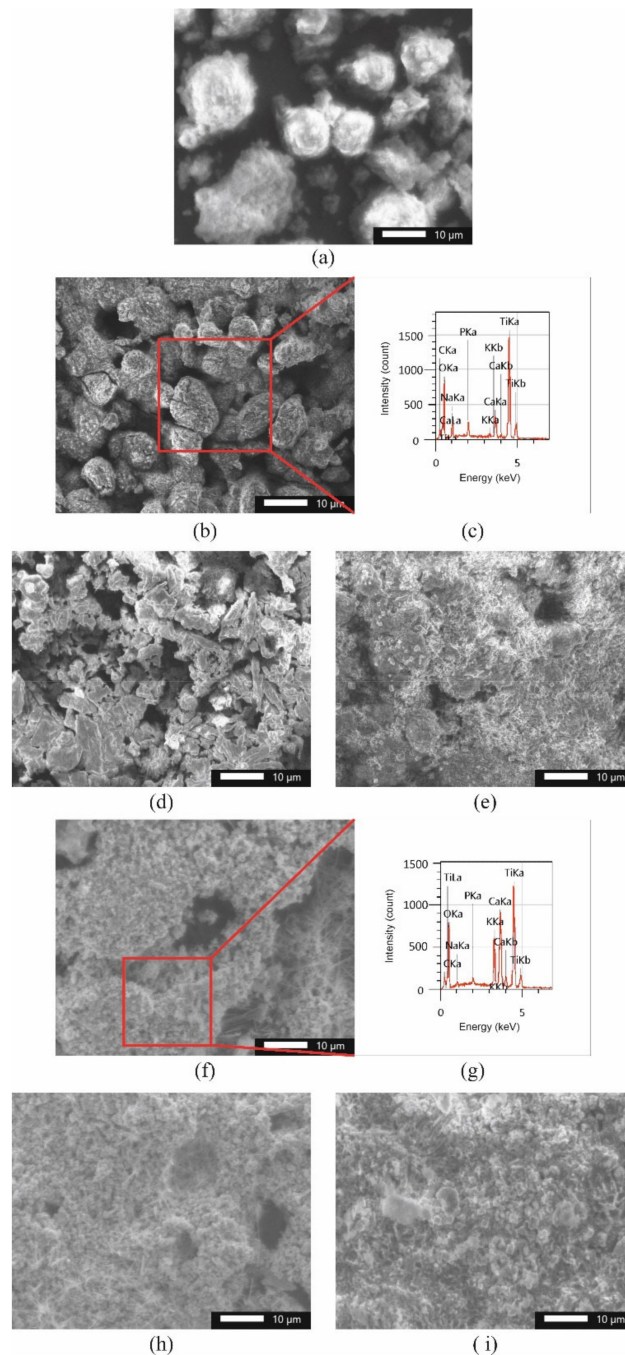
Figure 5. Scanning electron microscopy (SEM): (**a**) shellac-coated hydroxyapatite before sintering; Ti-HA composites (**b**) S1, (**d**) S2, (**e**) S3, (**f**) S4, (**h**) S5, and (**i**) S6. Energy dispersive X-ray (EDX) analysis: (**c**) S1 and (**g**) S4.

3.2. Antibacterial Activities

The antibacterial activities of the Ti-HA composites were determined using the disc diffusion method, and the results can be seen in Figure 6. The chloramphenicol disc (D = 6 mm), used as a positive control (+), showed a large zone of inhibition against *Escherichia coli* (D = 34.05 ± 0.42 mm) and *Staphylococcus aureus* (D = 28.25 ± 0.35 mm) bacteria. The blank disc was used as a negative control (−). The inhibition zones for the Ti-HA composites are displayed in Figure 7.
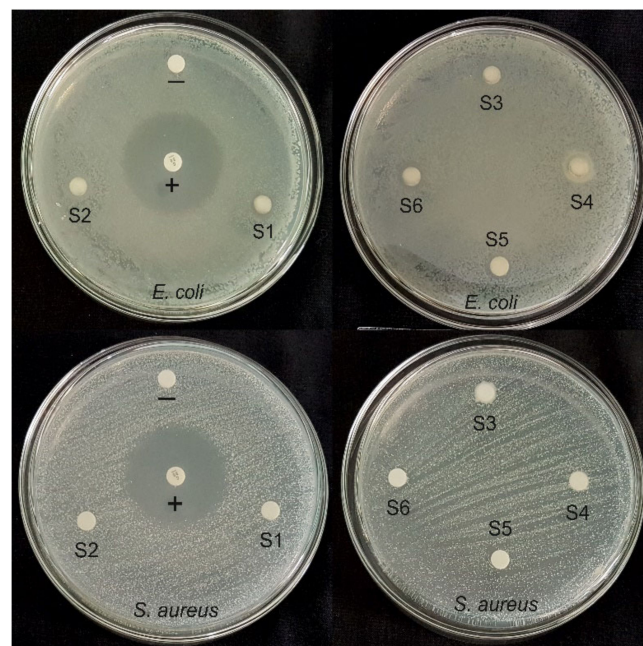
Figure 6. Zone of inhibition (ZOI): control positive (+); control negative (–); Ti-HA composites (S1–S6) against bacteria (*E. coli* and *S. aureus*).
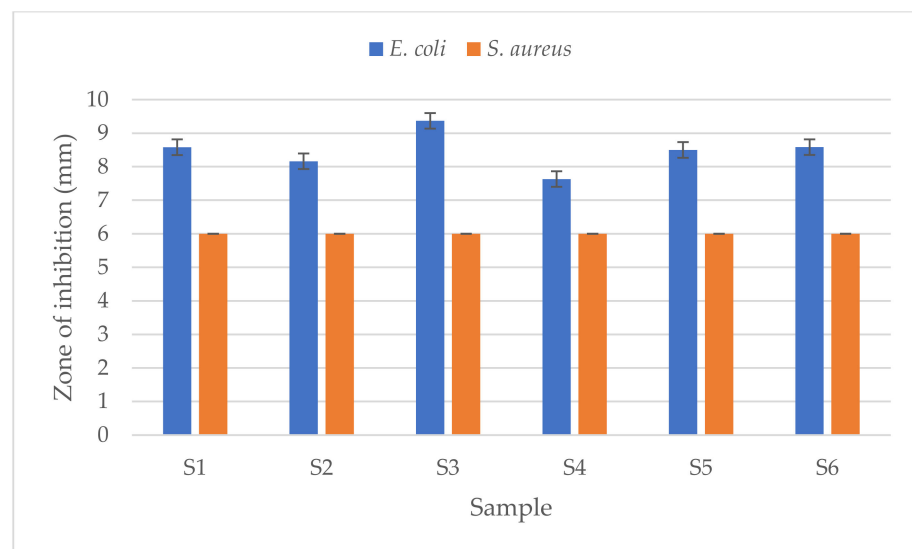

Figure 7. Zone of inhibition: Ti-HA composites (S1–S6) with concentrations of 100 mg/mL against *Escherichia coli* and *Staphylococcus aureus* bacteria.

The Ti-HA composites had a greater inhibition zone against *E. coli* than against *S. aureus* bacteria. The highest inhibition zone was seen against *E. coli*, including: 8.58 ± 0.66 mm for S1; 8.16 ± 0.81 mm for S2; 9.37 ± 0.26 mm for S3; 7.63 ± 1.18 mm for S4; 8.5 ± 0.51 mm for S5; and 8.58 ± 1.09 mm for S6 ($p < 0.05$), while the samples do not have antibacterial activity against *S. aureus*. The dissimilarity of the cell walls for gram-positive and gram-negative bacteria could be the cause of the different results for antibacterial activities [39]. *S. aureus* has a cell wall thickness between 20 and 80 nm, with two layers of peptidoglycan, whereas *E. coli* has a thinner cell wall of about 1.5–10 nm, with only one layer of peptidoglycan [20]. Because it has a thinner peptidoglycan layer, the mobilization of metal ion particles into the cells became easier and assists the interaction between the ion particles and the cell wall of bacteria. The lipopolysaccharide layer in gram-negative bacteria also has a role as an integrating factor for positive ions, which leads to particle emission and the destruction of DNA and proteins [40].

Titanium and hydroxyapatite have positively charged ions. A positive ion, also known as a cation, is an ion that has more protons than electrons. The structure of positively charged ions means that there is attraction when in contact with negative ions from microbes, due to an imbalance of ions. As a result, the cell walls that carry proteins will break. Positive ions will be attracted into the cell by the negative ions, disrupting the cellular systems for synthesis and metabolism until the bacterial microbes are killed [41].

The pH of the environment also changed after the incubation process. The initial pH of the medium was 7.3; after 24 h of incubation with sample concentrations of 100 mg/mL, the pH changed to 7.9 and 8.1 for the *S. aureus* and *E. coli* bacteria, respectively. Such pH changes are another way to prevent bacterial growth. Bacterial metabolism is influenced by such changes because of the alterations to the thermodynamic and kinetic properties of oxidation–reduction, which can change structures within the bacterial microorganism [42].

In this study, the Ti-HA composite was observed for antibacterial activity and showed an inhibition zone on *E. coli* bacteria. The inhibition zone formed in the area around the samples was caused by the presence of positive ions, which was known based on physicochemical characterization of the composite that interacts with the cell wall of gram-negative bacteria [40]. Nano-sized particles with the synthesis process showed good cell activity and easy degradation [43]. There is an opportunity to modify particle sizes into the nanoscale for further research with in vivo and clinical testing to ensure the biocompatibility of the Ti-HA composite.

4. Conclusions

Ti-HA composites were synthesized using a wet-precipitation method and shellac as a binder through sintering at 800 °C in air environmental conditions under varying holding times and powder compositions. It is known that shellac disappears during the sintering process, and this was confirmed by the lack of observed characteristic diffraction peaks for the composites. The phases that appeared were the initial phases and that of bonding between the two materials. The sintering time affected the crystallinity of the composites, as observed by the disappearance of diffraction peaks with increased holding time. Particle interconnection happened at 800 °C, meaning that micropores appeared on the composites. Furthermore, titanium bonded with oxygen in the air; thus, quite a lot of oxygen was found in all of the sintered composites. FTIR analysis confirmed the presence of carbonate, phosphate, and hydroxyl groups. Deconvolution was carried out to confirm type "AB" substitutions of carbonate groups into hydroxyl or phosphate groups. The Ti-HA composites had a larger inhibition zone against *E. coli* than against *S. aureus* bacteria. The difference in the zones of inhibition may be due to the differences in cell wall thickness between the two microorganisms. Additionally, pH changes that occurred after incubation for 24 h also affected the inhibition of bacterial growth. Antibacterial activity is a significant problem when implants are inserted into the human body, and this represents semiquantitative biocompatibility testing of this material. Further research is needed to determine the biocompatibility of Ti-HA composites quantitatively and in vivo.

Data Availability Statement: The data presented in this study are available from the corresponding author.

Conflicts of Interest: The authors declare no conflict of interest.

References

1. Diago, A.M.D.; Generali, L.; Apponi, R.; Colombini, V.; Checchi, V. Traumatic Dental Injuries: Clinical Case Presentation and a 10-Year Epidemiological Investigation in an Italian Dental Emergency Service. *Case Rep. Dent.* **2021**, *2021*, 86496632021. [CrossRef]
2. Zaleckiene, V.; Peciuliene, V.; Brukiene, V.; Drukteinis, S. Traumatic dental injuries: Etiology, prevalence and possible outcomes. *Stomatologija* **2014**, *16*, 7–14. [PubMed]
3. Wang, X.; Wan, C.; Feng, X.; Zhao, F.; Wang, H. In Vivo and In Vitro Analyses of Titanium-Hydroxyapatite Functionally Graded Material for Dental Implants. *BioMed Res. Int.* **2021**, *2021*, 8859945. [CrossRef] [PubMed]
4. Arifin, A.; Sulong, A.B.; Muhamad, N.; Syarif, J.; Ramli, M.I. Material processing of hydroxyapatite and titanium alloy (HA/Ti) composite as implant materials using powder metallurgy: A review. *Mater. Des.* **2014**, *55*, 165–175. [CrossRef]
5. Mondal, A.; Sohel, A.; Mohammed, A.P.; Anu, A.S.; Thomas, S.; Sengupta, A. Crystallization study of shellac investigated by differential scanning calorimetry. *Polym. Bull.* **2019**, *77*, 5127–5143. [CrossRef]
6. İzmir, M.; Ercan, B. Anodization of titanium alloys for orthopedic applications. *Front. Chem. Sci. Eng.* **2019**, *13*, 28–45. [CrossRef]
7. Hsu, H.-C.; Hsu, S.-K.; Wu, S.-C.; Wang, P.-H.; Ho, W.-F. Design and characterization of highly porous titanium foams with bioactive surface sintering in air. *J. Alloy. Compd.* **2013**, *575*, 326–332. [CrossRef]
8. Farias, K.A.S.; Sousa, W.J.B.; Cardoso, M.J.B.; Lima, R.J.S.; Rodriguez, M.A.; Fook, M.V.L. Obtaining hydroxyapatite with different precursors for application as a biomaterial. *Ceramica* **2019**, *65*, 99–106. [CrossRef]
9. Kumar, G.S.; Thamizhavel, A.; Girija, E. Microwave conversion of eggshells into flower-like hydroxyapatite nanostructure for biomedical applications. *Mater. Lett.* **2012**, *76*, 198–200. [CrossRef]
10. Biedrzycka, A.; Skwarek, E.; Osypiuk, D.; Cristóvao, B. Synthesis of Hydroxyapatite/Iron Oxide Composite and Comparison of Selected Structural, Surface, and Electrochemical Properties. *Materials* **2022**, *15*, 1139. [CrossRef]
11. Sazesh, S.; Ghassemi, A.; Ebrahimi, R.; Khodaei, M. Fabrication and characterization of nHA/titanium dental implant. *Mater. Res. Express* **2019**, *6*, 045060. [CrossRef]
12. Anawati; Tanigawa, H.; Asoh, H.; Ohno, T.; Kubota, M.; Ono, S. Electrochemical corrosion and bioactivity of titanium-hydroxyapatite composites prepared by spark plasma sintering. *Corros. Sci.* **2013**, *70*, 212–220. [CrossRef]
13. Arifin, A.; Sulong, A.B.; Muhamad, N.; Syarif, J.; Ramli, M.I. Powder injection molding of HA/Ti6Al4V composite using palm stearin as based binder for implant material. *Mater. Des.* **2015**, *65*, 1028–1034. [CrossRef]
14. Weththimuni, M.L.; Capsoni, D.; Malagodi, M.; Milanese, C.; Licchelli, M. Shellac/nanoparticles dispersions as protective materials for wood. *Appl. Phys. A Mater. Sci. Process* **2016**, *122*, 1058. [CrossRef]
15. Comín, R.; Cid, M.P.; Grinschpun, L.; Oldani, C.; Salvatierra, N.A. Titanium-Hydroxyapatite Composites Sintered at Low Temperature for Tissue Engineering: In vitro Cell Support and Biocompatibility. *J. Appl. Biomater. Funct. Mater.* **2017**, *15*, e176–e183. [CrossRef]
16. Lamkhao, S.; Phaya, M.; Jansakun, C.; Chandet, N.; Thongkorn, K.; Rujijanagul, G.; Bangrak, P.; Randorn, C. Synthesis of Hydroxyapatite with Antibacterial Properties Using a Microwave-Assisted Combustion Method. *Sci. Rep.* **2019**, *9*, 4015. [CrossRef]
17. Ashraf, R.; Sofi, H.S.; Akram, T.; Rather, H.A.; Abdal-Hay, A.; Shabir, N.; Vasita, R.; Alrokayan, S.H.; Khan, H.A.; Sheikh, F.A. Fabrication of multifunctional cellulose/TiO$_2$/Ag composite nanofibers scaffold with antibacterial and bioactivity properties for future tissue engineering applications. *J. Biomed. Mater. Res. Part A* **2020**, *108*, 947–962. [CrossRef]
18. Triyono, J.; Susmartini, S.; Susilowati, E.; Murdiyantara, S.A. Shellac Coated Hydroxyapatite (HA) Scaffold for Increasing Compression Strength. *Adv. Mater. Res.* **2015**, *1123*, 378–382. [CrossRef]
19. Parvizifard, M.; Karbasi, S.; Salehi, H.; Bakhtiari, S.S.E. Evaluation of physical, mechanical and biological properties of bio-glass/titania scaffold coated with poly (3-hydroxybutyrate)-chitosan for bone tissue engineering applications. *Mater. Technol.* **2019**, *35*, 75–91. [CrossRef]
20. Murugan, N.; Murugan, C.; Sundramoorthy, A.K. In vitro and in vivo characterization of mineralized hydroxyapatite/polycaprolactone-graphene oxide based bioactive multifunctional coating on Ti alloy for bone implant applications. *Arab. J. Chem.* **2018**, *11*, 959–969. [CrossRef]
21. Peng, Q.; Bin, X.; Xuxing, H.; Wang, Y.; Peng, Z.; Tang, Z. Facile fabrication of boronized Ti6Al4V/HA composites for load-bearing applications. *J. Alloy. Compd.* **2020**, *825*, 153102. [CrossRef]
22. Anaee, R.A. Behavior of Ti/HA in Saliva at Different Temperatures as Restorative Materials. *J. Bio Tribo Corros.* **2016**, *2*, 5. [CrossRef]
23. Mondal, D.; Patel, M.; Jain, H.; Jha, A.; Das, S.; Dasgupta, R. The effect of the particle shape and strain rate on microstructure and compressive deformation response of pure Ti-foam made using acrowax as space holder. *Mater. Sci. Eng. A* **2014**, *625*, 331–342. [CrossRef]
24. Kumar, C.G.; Pombala, S.; Poornachandra, Y.; Agarwal, S.V. Synthesis, characterization, and applications of nanobiomaterials for antimicrobial therapy. *Nanobio Mater. Antimicrob. Ther.* **2016**, *6*, 103–152. [CrossRef]

25. Aygul, E.; Yalcinkaya, S.; Sahin, Y. Microstructural analysis of sintered pure-titanium and titanium/hydroxyapatite (HA) surgical implant materials under different temperatures and HA doped conditions produced by powder metallurgy. *Mater. Res. Express* **2020**, *7*, 035402. [CrossRef]

26. Sarkar, P.; Shrivastava, A. FTIR spectroscopy of lac resin and its derivatives. *Pigment Resin Technol.* **1997**, *26*, 378–381. [CrossRef]

27. Stevanović, M.; Djošić, M.; Janković, A.; Kojić, V.; Vukašinović-Sekulić, M.; Stojanović, J.; Odović, J.; Sakač, M.C.; Yop, R.K.; Mišković-Stanković, V. Antibacterial graphene-based hydroxyapatite/chitosan coating with gentamicin for potential applications in bone tissue engineering. *J. Biomed. Mater. Res. Part A* **2020**, *108*, 2175–2189. [CrossRef]

28. Enayati-Jazi, M.; Solati-Hashjin, M.; Nemati, A.; Bakhshi, F. Synthesis and characterization of hydroxyapatite/titania nanocomposites using in situ precipitation technique. *Superlattices Microstruct.* **2012**, *51*, 877–885. [CrossRef]

29. Artimani, J.S.; Ardjmand, M.; Enhessari, M.; Javanbakht, M. Polybenzimidazole/BaCe0.85Y0.15O3-δ nanocomposites with enhanced proton conductivity for high-temperature PEMFC application. *Can. J. Chem.* **2019**, *97*, 520–528. [CrossRef]

30. Ye, H.; Liu, X.Y.; Hong, H. Characterization of sintered titanium/hydroxyapatite biocomposite using FTIR spectroscopy. *J. Mater. Sci. Mater. Electron.* **2008**, *20*, 843–850. [CrossRef]

31. Yılmaz, E.; Kabataş, F.; Gökçe, A.; Fındık, F. Production and Characterization of a Bone-Like Porous Ti/Ti-Hydroxyapatite Functionally Graded Material. *J. Mater. Eng. Perform.* **2020**, *29*, 6455–6467. [CrossRef]

32. Brangule, A.; Gross, K.A. Importance of FTIR Spectra Deconvolution for the Analysis of Amorphous Calcium Phosphates. *IOP Conf. Ser. Mater. Sci. Eng.* **2015**, *77*, 012027. [CrossRef]

33. Wibowo, W.; Lenggana, B.W.; Ubaidillah, U.; Ariawan, D.; Imaduddin, F.; Mazlan, S.A.; Choi, S.-B. Declining Performance of Silicone-Based Magnetorheological Elastomers after Accelerated Weathering. *Materials* **2021**, *14*, 6389. [CrossRef] [PubMed]

34. Pastero, L.; Bruno, M.; Aquilano, D. About the Genetic Mechanisms of Apatites: A Survey on the Methodological Approaches. *Minerals* **2017**, *7*, 139. [CrossRef]

35. Fleet, M.E.; Liu, X. Location of type B carbonate ion in type A–B carbonate apatite synthesized at high pressure. *J. Solid State Chem.* **2004**, *177*, 3174–3182. [CrossRef]

36. Laskus, A.; Kolmas, J. Ionic Substitutions in Non-Apatitic Calcium Phosphates. *Int. J. Mol. Sci.* **2017**, *18*, 2542. [CrossRef]

37. Bovand, D.; Yousefpour, M.; Rasouli, S.; Bagherifard, S.; Bovand, N.; Tamayol, A. Characterization of Ti-HA composite fabricated by mechanical alloying. *Mater. Des.* **2015**, *65*, 447–453. [CrossRef]

38. Niespodziana, K.; Jurczyk, K.; Jakubowicz, J.; Jurczyk, M. Fabrication and properties of titanium–hydroxyapatite nanocomposites. *Mater. Chem. Phys.* **2010**, *123*, 160–165. [CrossRef]

39. Tamer, T.M. Development of polyvinyl alcohol/kaolin sponges stimulated by marjoram as hemostatic, antibacterial, and antioxidant dressings for wound healing promotion. *Int. J. Mol. Sci.* **2021**, *22*, 13050. [CrossRef]

40. Azizi-Lalabadi, M.; Ehsani, A.; Divband, B.; Alizadeh-Sani, M. Antimicrobial activity of Titanium dioxide and Zinc oxide nanoparticles supported in 4A zeolite and evaluation the morphological characteristic. *Sci. Rep.* **2019**, *9*, 7439. [CrossRef]

41. Dhanker, R.; Hussain, T.; Tyagi, P.; Singh, K.T.; Kamble, S.S. The Emerging Trend of Bio-Engineering Approaches for Microbial Nanomaterial Synthesis and Its Applications. *Front. Microbiol.* **2021**, *12*, 638003. [CrossRef] [PubMed]

42. Choudhary, R.; Venkatraman, S.K.; Chatterjee, A.; Vecstaudza, J.; Yáñez-Gascón, M.J.; Pérez-Sánchez, H.; Locs, J.; Abraham, J.; Swamiappan, S. Biomineralization, antibacterial activity and mechanical properties of biowaste derived diopside nanopowders. *Adv. Powder Technol.* **2019**, *30*, 1950–1964. [CrossRef]

43. Biedrzycka, A.; Skwarek, E.; Hanna, U.M. Hydroxyapatite with magnetic core: Synthesis methods, properties, adsorption and medical applications. *Adv. Colloid Interface Sci.* **2021**, *291*, 102401. [CrossRef] [PubMed]